CODEN IEJMAT *Internet Electronic Journal of Molecular Design* **2005**, *4*, 721–736 ISSN 1538–6414
BioChem Press http://www.biochempress.com

Inter*net* Electronic Journal of
Molecular Design

October 2005, Volume 4, Number 10, Pages 721–736

Editor: Ovidiu Ivanciuc

Proceedings of the Internet Electronic Conference of Molecular Design 2004
IECMD 2004, November 29 – December 12, 2004

Study of the Glass Transition Temperatures of Stereoregular PMMAs Using Different Force Fields

Armand Soldera and Noureddine Metatla

Département de Chimie, Université de Sherbrooke, Sherbrooke, J1K 2R1, Canada

Received: November 2, 2004; Revised: January 27, 2005; Accepted: May 6, 2005; Published: October 31, 2005

Citation of the article:
A. Soldera and N. Metatla, Study of the Glass Transition Temperatures of Stereoregular PMMAs Using Different Force Fields, *Internet Electron. J. Mol. Des.* **2005**, *4*, 721–736, http://www.biochempress.com.

Inter*net* Electronic Journal of Molecular Design

BioChem Press
http://www.biochempress.com

Study of the Glass Transition Temperatures of Stereoregular PMMAs Using Different Force Fields

Armand Soldera* and Noureddine Metatla

Département de Chimie, Université de Sherbrooke, Sherbrooke, J1K 2R1, Canada

Received: November 2, 2004; Revised: January 27, 2005; Accepted: May 6, 2005; Published: October 31, 2005

Internet Electron. J. Mol. Des. **2005**, *4* (10), 721–736

Abstract

Motivation. Poly(methyl methacrylate), PMMA, offers a particular regard to the study of the glass transition since according to the tacticity of its chain, a different glass temperature transition, T_g, is exhibited. Molecular modeling is thus a perfect tool to study such a variation since changes that occur during these transitions can be regarded as differences in molecular characteristics only. The selection of a forcefield that correctly depicts this difference is thus of primary importance. In this article, two forcefields, AMBER and AMBER/OPLS, have been used to simulate the glass transition of the stereoregular PMMAs. Results stemming from these simulations are compared with those, already published, coming from a second generation force field, *pcff*.

Method. Molecular dynamics simulations are used to study the glass transition of stereoregular polymers, and their energetic differences, with respect to the use of two force fields of different generation.

Results. Although T_gs are obtained at higher temperatures than those obtained with the *pcff* force field, the difference between the two T_gs is better mimicked using the AMBER/OPLS force field. The presence of the cross terms in the force fields is thus not a determining factor in getting the T_gs variation. A first generation force field could deal with the representation of the difference in T_gs between stereoregular polymers.

Conclusions. Accordingly to the fact that a first generation force field can deal with the difference in T_gs difference, a greater amount of phase space could be regarded. Moreover, studies of specific interaction, such as PMMA behavior with surfaces, can be undertaken.

Keywords. Glass transition temperature; steroregular poly(methylmethacrylate); AMBER/OPLS; molecular dynamics.

Abbreviations and notations

PMMA, poly(methylmethacrylate)	QEq, method of charge equilibration
i–PMMA, isotactic PMMA	s–PMMA, syndiotactic PMMA

1 INTRODUCTION

Molecular modeling of polymers is becoming more and more relevant for industrial applications and academic researches. Such an increase stems from different factors: increase of computer efficiency, availability of commercial codes with attractive environment, and improvement of force

Presented in part at the Internet Electronic Conference of Molecular Design 2004, IECMD 2004.

* Correspondence author; phone: +1–819–821–7650; fax: +1–819–821–8017; E–mail: Armand.Soldera@Usherbrooke.ca.

fields. The choice of a force field could have dramatic effect on the value of the final properties. Nevertheless with present second category force field such as COMPASS [1], MM4 [2], the probability that an atom is not correctly documented has considerably decreased. Such a high transferability is not always requested. The use of a first category force field where there is no cross–term, has several advantages. Each term of the mathematical formulation of the force field possesses its own physical significance. Moreover, less CPU (Central Process Unit) time is requested. For instance considering a specific system, the CPU time requested for a simulation using a first category force field is reduced by a factor of 4 comparatively to the time needed for the same simulation using the second category force field, *pcff*. Moreover, it has to be pointed out that the physical significance of the cross–terms inside a second category force field is still a source of debate [3]. In the perspective to a better understanding of the differences between stereoregular PMMAs, the physical significance of each mathematical term inside a force field is a relevant parameter. Using a first generation force field also shows an attractive aspect regarding to the phase space that can be explored since a less amount of CPU time is needed. Consequently, a better description of the property of interest can be claimed.

Poly(methyl methacrylate), PMMA, whose repeat unit is displayed in Figure 1, is an ideal polymer to study physical properties using molecular modeling. According to the tacticity of its chain, different experimental properties are exhibited: solubilities, crystal structures [4]. The property of interest of the studies reported in this article is the glass transition temperature, T_g.

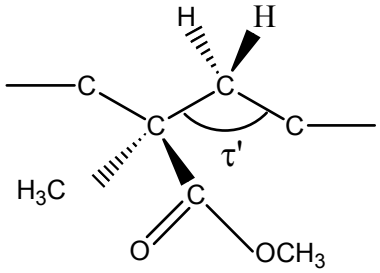

Figure 1. PMMA repeat unit.

Using molecular simulation the difference in the T_gs between the two PMMA configurations can be regarded as changes in molecular characteristics only. As a matter of fact, if a force field appropriately deals with such differences, insights on the reasons that give rise to these variations can be gained. Actually the tricky problem of the glass transition itself can also be envisioned. Several studies have been carried out using the second category force field, *pcff* [5-8]. However, the glass transition difference has not been yet observed using a first category force field. In fact, several studies on PMMA have been concerned by the use of a first class force field [9,10], but the difference in properties of the two PMMA configurations has only been addressed by the AMBER force field [4]. The computed property was the solubility parameter. A question then arises: can a first category force field deal with the difference in T_gs? The purpose of this article is to address this

question, and thus to propose a first category force field that will be used in subsequent studies to investigate more deeply the difference in the T_gs.

2 SIMULATION METHODS

2.1 Force field

Due to the great number of atoms in polymer chains, empirical methods, that are molecular mechanics and dynamics, are currently used to deal with polymer simulation. Both methods are based on the use of a force field. The accuracy of a force field used during a simulation has a great impact on the final results. Several factors can affect its efficiency. A force field actually expresses in average the electronic interactions between atoms [11]. Its mathematical formulation has thus to include all these interactions, where each mathematical term possesses its own physical significance. A series of data is then obtained from the fit of these equations to experimental or *ab initio* data. Differences between the force fields stem from the expression of these equations and their parameterization. The equations could differ from the degree of their Taylor expansion, or from their functional form. For instance, the covalent bond can be depicted by a Morse function, a Hooke's law, a quartic equation, or a higher Taylor expansion of the Morse function (MM4) [2]. The ensemble of the parameterization data associated with an atom in a specific environment is called a potential. The great variety of electronic environments of an atom yields to numerous potentials for this atom. In fact, the number of these potentials for an atom differs among the force fields. A high transferability force field possesses numerous potentials for an atom; for instance the carbon atom possesses 20 different potentials in the *pcff* force field [12]. A force field is thus defined by its mathematical expression and the list of the atomic potentials [13]. As a matter of fact, the building of a force field is a difficult task that needs particular attention. Since the goal of the studies reported in this article was to find a first class force field to accurately mimic the difference in T_gs between the two PMMA configurations, only existing force fields were regarded.

The equation of a force field is usually split into the intramolecular part which takes into account the connectivity and the flexibility of the polymer chains, and the intermolecular part, or non–bond terms, which is constituted by a repulsive, a dispersive and an electrostatic terms. A classification is also made among the force fields by considering the presence or not of cross–terms in the intramolecular part. A force field which possesses these additional term is said to be of second category force field [3]. The efficiency to depict the difference in T_gs between the two PMMA configurations by such a force field, *pcff*, has already been shown [12]. Are these off–diagonal terms relevant to describe this variation is a question that this article will attempt to answer.

Two first category force fields were considered. They both come from the AMBER force field [14]. The AMBER force field was the force field used to study the difference in the solubility

parameters between the two PMMA configurations [4]. Besides the AMBER force field, AMBER/OPLS was also chosen to simulate the variation in T_gs in PMMA chains. The difference between the two force fields is the way the partial charges that are included in the electrostatic potential were computed. It has to be pointed out that DREIDING, a first class force field, was used to simulate the PMMA configurations; but both PMMA configurations were studied separately [10,15].

The mathematical expressions of the first generation force fields (AMBER or AMBER/OPLS) and *pcff* are shown in Eq. (1) and (2), respectively.

$$\begin{aligned} V = & \sum_b K\left(b-b_0\right)^2 + \sum_\theta H\left(\theta-\theta_0\right)^2 \\ & + \sum_\phi \left[V_1\left[1-\cos\left(\phi-\phi_1^0\right)\right] + V_2\left[1-\cos\left(2\phi-\phi_2^0\right)\right] + V_3\left[1-\cos\left(3\phi-\phi_3^0\right)\right]\right] \\ & + \sum_{i>j} \frac{q_i q_j}{\varepsilon r_{ij}} + \sum_{i>j} 4\varepsilon_{ij}\left[\left(\frac{\sigma_{ij}}{r_{ij}}\right)^{12} - \left(\frac{\sigma_{ij}}{r_{ij}}\right)^{6}\right] \end{aligned} \tag{1}$$

where K, H, V_1, V_2, V_3, b_0, θ_0, ϕ_1^0, ϕ_2^0, ϕ_3^0, ε_{ij}, σ_{ij}, q_i, and q_j are potential parameters included into the force field. b, θ, ϕ, and r_{ij} are bond length, valence angle, dihedral angle, and non–bonding distance between two atoms i and j, respectively. These parameters are acquired during simulation, and are used to compute the energetical values that are reported in this paper.

$$\begin{aligned} V = & \sum_b \left[K_2\left(b-b_0\right)^2 + K_3\left(b-b_0\right)^3 + K_4\left(b-b_0\right)^4\right] + \sum_\theta \left[H_2\left(\theta-\theta_0\right)^2 + H_3\left(\theta-\theta_0\right)^3 + H_4\left(\theta-\theta_0\right)^4\right] \\ & + \sum_\phi \left[V_1\left[1-\cos\left(\phi-\phi_1^0\right)\right] + V_2\left[1-\cos\left(2\phi-\phi_2^0\right)\right] + V_3\left[1-\cos\left(3\phi-\phi_3^0\right)\right]\right] + \sum_\chi K_\chi \chi^2 \\ & + \sum_b \sum_{b'} F_{bb'}\left(b-b_0\right)\left(b'-b'_0\right) + \sum_\theta \sum_{\theta'} F_{\theta\theta'}\left(\theta-\theta_0\right)\left(\theta'-\theta'_0\right) + \sum_b \sum_\theta F_{b\theta}\left(b-b_0\right)\left(\theta-\theta_0\right) \\ & + \sum_b \sum_\phi \left(b-b_0\right)\left[V_1\cos\phi + V_2\cos 2\phi + V_3\cos 3\phi\right] + \sum_{b'} \sum_\phi \left(b'-b'_0\right)\left[V_1\cos\phi + V_2\cos 2\phi + V_3\cos 3\phi\right] \\ & + \sum_\theta \sum_\phi \left(\theta-\theta_0\right)\left[V_1\cos\phi + V_2\cos 2\phi + V_3\cos 3\phi\right] + \sum_\phi \sum_\theta \sum_{\theta'} K_{\phi\theta\theta'}\cos\phi\left(\theta-\theta_0\right)\left(\theta'-\theta'_0\right) \\ & + \sum_{i>j} \frac{q_i q_j}{\varepsilon r_{ij}} + \sum_{i>j} \varepsilon_{ij}\left[2\left(\frac{r^*_{ij}}{r_{ij}}\right)^9 - 3\left(\frac{r^*_{ij}}{r_{ij}}\right)^6\right] \end{aligned} \tag{2}$$

where K_2, K_3, K_4, H_2, H_3, H_4, V_1, V_2, V_3, b_0, b'_0, θ_0, θ'_0, $F_{bb'}$, $F_{\theta\theta'}$, $F_{b\theta}$, ϕ_1^0, ϕ_2^0, ϕ_3^0, ε_{ij}, r^*_{ij}, q_i, and q_j are potential parameters included into the force field. b (b'), θ (θ'), ϕ, and r_{ij} are bond length, valence angle, dihedral angle, and non–bonding distance between two atoms i and j, respectively. These parameters are acquired during simulation.

Potential parameters used during the simulations are indicated in the appendixes: Appendix 1 for the non–bonding term, Appendix 2 for the partial charges of the electrostatic term, Appendix 3 for the bonding term, Appendix 4 for the valence angle term, and Appendix 5 for the torsion term. The AMBER type convention is used for all potentials i.e. those used for the AMBER, AMBER/OPLS, and *pcff* force fields: CT = sp^3 carbon, C = carbonyl carbon, HC = hydrogen attached to carbon, O =

carbonyl oxygen, OS = ethyl and ester oxygen. Since the potential parameters associated with the cross terms are not relevant to these studies, they are not shown.

Regarding the partial charges, two sets were used. The first set corresponds to the AMBER force field partial charges that have been used to compute the solubility parameters of the two PMMA configurations [4]. These charges were determined from the crystal structure of PMMA. The second set is the OPLS partial charges [16]. The OPLS charges were established to fit experimental density and vaporization enthalpies. They accurately simulate the liquids.

2.2 Computer Software

An important step in the molecular modeling of polymers is the accurate representation of the phase space. Since the ergodic hypothesis is never fulfilled, a specific procedure has to be carried out to correctly depict the configurational space related to the polymer chain configuration in the bulk. The choice of the configurations embedded in a cell with periodic boundary conditions [17] is therefore crucial. A polymer chain with one hundred repeat units (RU) propagates into the periodic box according to the self–avoiding walk algorithm [18], considering the long–range non–bonded interactions described by Theodorou and Suter [19]. The procedure is implemented in the Accelrys *Amorphous_Cell*© software. The detailed procedure can be found in [5]. Thirty configurations were initially generated using the *pcff* force field. The end–to–end distances were computed: 51 ± 10 Å, and 33 ± 10 Å, for i–PMMA, and s–PMMA, respectively. The higher value of the end–to–end distance for i–PMMA is in agreement with expected values [20]. Configurations that possess an end–to–end distance which departs too much from the average value were not considered in the simulations. A relaxation procedure (molecular dynamics and minimization) was then undertaken with the remaining configurations. Ten configurations which exhibit the lowest energy were thus obtained, and were used to simulate the glass transition. The procedure was repeated for each chain tacticity.

To perform molecular dynamics, MD, simulations, the DL_POLY code was used [21]. The leap–frog variant of the velocity Verlet algorithm was used to integrate the Newtonian equations of motion, with an integration step of 0.001 ps. The duration of the MD simulation for each data reported in the dilatometric curves was 110 ps (10 ps of equilibration in the NVT ensemble). During MD simulations with the AMBER and AMBER/OPLS force fields, Berendsen thermostat and barostat were used to keep the system at desired temperatures and pressures, respectively [22]. It has to be mentioned that in the simulations involving the *pcff* force field the temperature was imposed in the primary step by the velocity–scaling algorithm, and then by the Andersen algorithm [23], and the pressure was controlled by the Parrinello–Rahman algorithm [24]. The non–bonded interactions were computed using the Ewald summation; a non–bond cut–off of 10 Å was chosen.

2.3 Dilatometric Simulation

The simulated dilatometry technique was used to determine the T_g [25]. The specific volume, *i.e*., the inverse of the density, is reported with respect to the temperature (Figures 2 and 3). The intercept of the lines joining the points of the two phases, the vitreous and rubbery, yields the value of the T_g. In order to get the specific volume at a desired temperature, MD simulations were performed in the NPT statistical ensemble, *i.e*., constant number of particles, pressure and temperature.

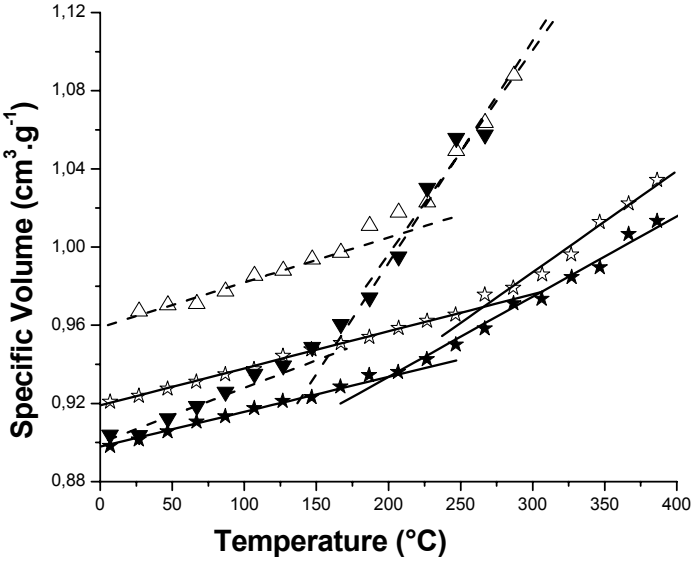

Figure 2. Simulated dilatometric curves for the two PMMA configurations according to two force fields: i–PMMA (▼), and s–PMMA (△) through the *pcff* force field simulation, and i–PMMA (★), and s–PMMA (☆) through the AMBER force field simulation.

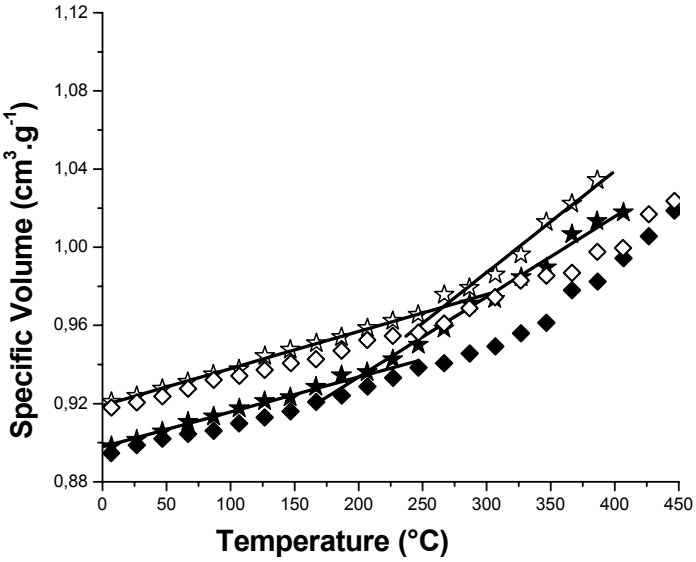

Figure 3. Simulated dilatometric curves for the two PMMA configurations according to two first category force fields: i–PMMA (◆), and s–PMMA (◇) through the AMBER force field simulation, and i–PMMA (★), and s–PMMA (☆) through the AMBER/OPLS force field simulation.

3 RESULTS AND DISCUSSION

3.1 Simulated Dilatometric Results

Simulated dilatometric curves of the PMMA configurations are displayed in Figures 2 and 3. The curves stemming from the simulations using the AMBER/OPLS force field are used as the reference. They are thus compared to those coming from simulations generated with the *pcff* and AMBER force fields, in Figures 2 and 3, respectively. It has to be pointed out, that with a view to clarity, standard deviations are not shown (in order of 0.005 g cm^{-3} below T_g and 0.01 g cm^{-3} above T_g), and dilatometric curves are not displayed in the same graph. The values of the T_gs for both PMMA configurations and their difference are thus compared to experimental data in Table 1.

Table 1. Experimental and simulated glass transition temperatures using the different force fields described in the text, for both PMMA configurations

Force field	T_g (i–PMMA) (°C)	T_g (s–PMMA) (°C)	ΔT_g
pcff	157	212	55
AMBER	322	338	16
AMBER/OPLS	201	265	64
Experimental	45	114	69

From Table 1, the values of the T_gs are clearly found superior than the experimental ones. Such a difference could be explained from two viewpoints. Firstly, the quenching rate is in order of 10^9 times more rapid than an experimental quenching rate. According to the time–temperature superposition principle, the T_g has to be higher than the experimental one [26]. Moreover, considering that a configuration was generated in the vitreous state, its thermal equilibrium at higher temperatures has to take a very long time [27]. However, it is argued that since the difference in T_gs is clearly reproduced, and that the portion of the phase space of interest is well represented, obtaining accurate absolute values is not critical for the physical interpretation of the glass transition phenomenon. Additionally, the fact that the T_g values using the AMBER/OPLS force field are found superior to those obtained from simulations with *pcff* force field, is explained by the difference in the value of the dihedral potential as mentioned by Boyd *et al.*: higher is the dihedral potential, higher is the T_g [28]. As reported in Appendix 5, a cross–barrier energy for a torsion along the backbone in the AMBER/OPLS force field is 0.50 kcal mol^{-1} higher than in the *pcff* force field. Accordingly, more thermal energy has to be brought to cross the energetic barrier, and thus according to the free volume theory higher is the T_g. However, the determination of the T_g values using AMBER is not rigorous, as it can be observed in Figure 3: a great range of transition temperatures could actually be obtained. Consequently, a difference in T_gs cannot be clearly identified. Unlike AMBER, T_gs can be extracted from dilatometric curves using *pcff* and AMBER/OPLS (Figure 2). Differences in T_gs between the two PMMA configurations can thus be achieved: 54°C for *pcff*, and 64°C for AMBER/OPLS. These values have to be compared with the 69°C experimentally obtained. It has to be mentioned that the experimental difference takes into

account the mass of the simulated polymer through the use of the Fox–Flory equation [5]. The better representation of this difference by the AMBER/OPLS force field could be explained by the better representation of the phase space.

Besides, the T_g values, the volumetric thermal coefficient, α, can also be extracted from dilatometric curves. For both first category force fields, comparable values of α are found. As a matter of fact, only values of α coming from the simulations using the AMBER/OPLS and *pcff* force fields, were compared to the experimental ones in Table 2 [5]. In the vitreous state, the α coefficient is slightly underestimated in the case of simulation using the AMBER/OPLS force field comparatively to the experimental data. In the rubbery state, it is also slightly below the experimental value, but in the case of the *pcff* force field, the coefficient is two times the experimental value. As suggested by Fan *et al*., the increase of uncertainties could be responsible for the discrepancy of the α value noticed at temperatures above T_g [29]. Another explanation stays in the poor representation of the phase space. In fact, once the configurational space has been selected, all the MD trajectories at different temperatures are restrained around these points in the phase space. In the rubbery phase, a greater amount of the phase space has to be explored since the entropy drastically increases. With AMBER/OPLS more configurations are generated. Consequently the phase space is better represented, and thus the values of α are found closer to the experimental data. Finally, the difference in the specific volume between the two PMMA configurations obtained using the AMBER/OPLS force field, 0.02 $cm^3\ g^{-1}$, is in the same order than the experimental one, 0.018 $cm^3\ g^{-1}$ [30].

Table 2. Simulated volumetric thermal expansion coefficients, α, using the AMBER/OPLS and *pcff* force fields, and experimental ones, for both PMMA configurations, in the vitreous and rubbery phases

State	Configuration	Experimental	pcff	AMBER/OPLS
vitreous	i–PMMA	$2.7\times10^{-4}\ K^{-1}$	$3.0\times10^{-4}\ K^{-1}$	$2.0\times10^{-4}\ K^{-1}$
	at–PMMA			
	s–PMMA		$2.4\times10^{-4}\ K^{-1}$	$2.0\times10^{-4}\ K^{-1}$
rubbery	i–PMMA	$5.7\times10^{-4}\ K^{-1}$	$11.0\times10^{-4}\ K^{-1}$	$4.2\times10^{-4}\ K^{-1}$
	at–PMMA			
	s–PMMA		$10.0\times10^{-4}\ K^{-1}$	$5.2\times10^{-4}\ K^{-1}$

Despite the values of T_gs that are found higher than the experimental ones, molecular modeling can deal with the difference in the glass transition temperatures between the two PMMA configurations for both category force fields. Nevertheless in the case of the first category force field simulations using the effective charges that derive from experimental data obtained with liquids show a better representation of the glass transition than the simulations with charges extracted from computational methods. Since charges with AMBER (QEq, *i.e*. charge equilibration) were computed from the PMMA crystal structure [4], they were not adapted to simulate the "liquid" like behavior. Since OPLS charges yield to accurate results, variations of the QEq charge values have not been undertaken. Considering the fact that the simulated T_gs were not determined with a

good accuracy, simulations with the AMBER force field was not considered in the property analyses.

3.2 Properties

A complete energetical description of the two PMMA configurations using the *pcff* force field was already described [6]. The attention was thus focused on the differentiation between the two category force fields simulation results.

Non–bonding energy. The intermolecular energy was found higher for the syndiotactic chains than for the isotactic chains whatever the category of force fields used: the difference was 20 kcal mol^{-1}, and 35 kcal mol^{-1} for the AMBER/OPLS and the *pcff* force fields, respectively [6]. The higher value for s–PMMA explains its lower density comparatively to the i–PMMA chain (Figure 3). Such a behavior agrees with the free volume theory to explain the difference in the T_gs. Higher is the non–bond energy, lower is the ability of the chain to crossover the energetic barrier, and thus to move more easily, and thus higher is the T_g. However, this difference could not explain the important variation of T_gs between the two PMMA configurations. Moreover, the greater difference in the non–bond energy found in *pcff* simulations compared with AMBER/OPLS simulations is not in accordance with the observed lower difference in the T_gs (Table 1). Further energetical analyses have thus to be pursued.

Intramolecular energy. Simulations using the two force fields exhibit a difference in the intramolecular energy between the two PMMA configurations: 45, and 72 kcal mol^{-1}, for *pcff* and AMBER/OPLS force fields, respectively. For both kinds of simulation, the dominant difference in intramolecular energy terms comes from the valence angle term [6]. The two other non–cross terms, the bonding and dihedral energy functions, do not exhibit significant differences. The variation in the valence energy between the two PMMA configurations is different: 75, and 35 kcal mol^{-1} for *pcff*, and AMBER/OPLS force fields, respectively.

To determine the angle responsible for this difference, all the valence angles were regarded; the procedure was published elsewhere [6]. A slight difference was observed between both force fields simulation results. Since the backbone valence angles contribute the most to the difference in the valence angle energy, they are shown in Table 3. Actually, the major contribution to the difference in the valence angle energy between the two PMMA configurations stems from the difference in the intra–diade angle (τ' in Figure 1). This important aperture arises in order to lessen the side–chain interactions [20]. Interactions between side–chains in a racemic diade are lower than in a meso diade, the aperture is thus less important for s–PMMA than for i–PMMA. This variation is observed for both force fields but values are different: 1.1 deg. and 0.6 deg. of difference for *pcff* and AMBER/OPLS, respectively. This difference is intrinsically linked to the difference in the valence energy, reported above. From Appendix 4, the equilibrium value of a CT–CT–CT angle (CT

corresponds to an sp^3 atom in the AMBER notation of atomic potentials) varies according to the force field: 112.67° in the case of *pcff*, and 109.5° for AMBER/OPLS. Consequently, in simulation using AMBER/OPLS more energy has to be brought in order to open the intradiade angle than in simulations with *pcff*. This could explain the difference in the valence energy observed between the different force field simulations.

Table 3. Comparison of the backbone angles between the force fields described in the text, for both PMMA configurations.

Angle	Configuration	Pcff	AMBER/OPLS
Intra–diade (τ')	i–PMMA	127.8 ± 0.1	128.7 ± 0.05
	s–PMMA	126.6 ± 0.1	128.1 ± 0.1
Inter–diade (τ)	i–PMMA	106.7 ± 0.2	108.7 ± 0.4
	s–PMMA	106.6 ± 0.2	108.3 ± 0.2

According to the free volume theory, higher is the non–bond energy, higher is the T_g; and greater is the backbone angle aperture, higher is the mobility of the chain, and thus lower is the T_g. The higher non–bond energy backbone angle aperture differences between the two PMMA configurations is observed in simulations using the *pcff* force field. Nevertheless the greater difference in T_gs is found in simulation with AMBER/OPLS force field. However, the highest values of the T_gs are obtained with AMBER/OPLS simulations. Accordingly thermal energy brought to the system tends to increase more the separation in the T_gs. A specific study on the mobility of the different chains has thus to be pursued. The question then arises on the way the thermal motion affects the side–chain mobility. Does it increase the rotation of the side–chain for the syndiotactic configuration, or decrease it in the case of the isotactic configuration? As can be observed by the study of the local dynamics using the *pcff* force field, the rotation of the side–chain greatly influences the mobility of the backbone, and thus the difference in T_gs between the two PMMA configurations [8]. Consequently, the energetical differences and the variations between the results brought by simulations using the two force fields, can only give a glimpse to the explanation of the difference in T_gs between the two configurations. Such observation has to be confirmed by a local dynamics analysis.

Dilatometric and energetic results clearly show that the interpretation of the difference in T_gs between the two PMMA configurations is not affected by the elimination of cross terms in the force fields. One advantage of using a first category force field is that energetic representation is simplified. Less parameters are thus needed for further simulations of PMMA involving the glass transition phenomenon. Moreover, a better description of the phase space can be considered without requesting too much CPU time; the entropic contribution is thus better estimated and the quasi–ergodic hypothesis, although not satisfied, is better addressed. However, attention has to be particularly paid when dealing with a first category force field. In the case of the AMBER force field, it has been seen that the use of QEq charges greatly affects the value of the T_g. The origin of this discrepancy could be explained by the fact that these charges were computed for PMMA in its

crystalline form. Besides the high values of the T_g obtained by the AMBER/OPLS force field the difference in T_gs between the two configurations of PMMA is accurately reproduced. The glass transition variation can therefore be simulated by a first category force field.

4 CONCLUSIONS

Cross–terms in the mathematical formulation of the force field do not affect the simulation of the difference in the T_gs between the two PMMA configurations. Conclusions deduced from the simulations using the two category force fields, are similar. From an energetical analysis, the non–bond energy is found higher for the syndiotactic configuration, in agreement with the free volume theory. From a geometrical analysis, the backbone intra–diade angle is greater for the i–PMMA chains. The aperture of this angle is due to lessen the interactions of the side–chains. Nevertheless, the difference in T_gs using the first category force field AMBER/OPLS shows a better accuracy with experimental data, than in the case of simulation using the second category force field *pcff*, despite the fact that higher T_g values are obtained. This better agreement can be explained by a better phase space representation, that was permitted by a greater amount of CPU time available by the use of a first category force field. Consequently, further analyses on the reasons that give rise to the difference in T_gs between the two PMMA configurations, and that request a great portion of the phase space, can be undertaken, using the AMBER/OPLS force field.

Acknowledgment

The work has been possible through the financial support of the Natural Sciences and Engineering Research Council, NSERC, of Canada and Université de Sherbrooke, the computer facilities of the Réseau Québécois de Calcul Haute Performance, the Canada Foundation for Innovation, and the Institut Supérieur des Matériaux et Mécaniques Avancés du Mans. The authors also wish to thank Pr. Y. Grohens for fruitful scientific discussion, and Pr. A.–M. Tremblay for the use of its computer cluster, Elix2.

Appendix 1

Parameters for non–bonding energetic term; a) for AMBER; b) for *pcff* force fields. For clarity, the mathematical expression is presented.

a) AMBER/OPLS $4\varepsilon_{ij}\left[\left(\frac{\sigma_{ij}}{r_{ij}}\right)^{12}-\left(\frac{\sigma_{ij}}{r_{ij}}\right)^{6}\right]$ with $\varepsilon_{ij}=\left(\varepsilon_i\varepsilon_j\right)^{1/2}$ and $\sigma_{ij}=\left(\sigma_i\sigma_j\right)^{1/2}$

atoms	σ_i (Å)	ε_i (kcal.mol^{-1})	Ref.
CT	3.500	0.066	1
C	3.750	0.105	2
OS	3.000	0.170	2
O	2.960	0.210	2
HC	2.500	0.030	1

1) W. L. Jorgensen et al., *J. Am. Chem. Soc.*, **118**, 11225(1996); 2) M. L. P. Price et al., *J. Comp. Chem.*, **22**, 1340 (2001)

b) AMBER

$$\left[\frac{A_{ij}}{R_{ij}^{12}}-\frac{B_{ij}}{R_{ij}^{6}}\right] \text{ with } R_{ij}^{*}=R_i^{*}+R_j^{*},\ A_{ij}=\varepsilon_{ij}\left(R_{ij}^{*}\right)^{12},\ B_{ij}=2\varepsilon_{ij}\left(R_{ij}^{*}\right)^{6} \text{ and } \varepsilon_{ij}=\left(\varepsilon_i\varepsilon_j\right)^{1/2}$$

atoms	R*(Å)	ε_i (kcal.mol^{-1})
CT	1.9080	0.1094
C	1.9080	0.0860
OS	1.6837	0.170
O	1.6612	0.210
HC	1.4870	0.0157

W. D. Cornell et al., *J. Am. Chem. Soc.* **117**, 5179 (1997).

c) *pcff*: $\varepsilon_{ij}\left[2\left(\frac{r_{ij}^{*}}{r_{ij}}\right)^{9}-3\left(\frac{r_{ij}^{*}}{r_{ij}}\right)^{6}\right]$ with $\varepsilon_{ij}=2\left(\varepsilon_i\varepsilon_j\right)^{1/2}\frac{\left(r_i^{*}\right)^3\left(r_j^{*}\right)^3}{\left(r_i^{*}\right)^6+\left(r_j^{*}\right)^6}$ and $r_{ij}^{*}=\left(\frac{\left(r_i^{*}\right)^6+\left(r_j^{*}\right)^6}{2}\right)^{1/6}$

Atoms	r_i^{*} (Å)	ε_i (kcal.mol^{-1})
CT	4.010	0.054
C	3.810	0.120
OS	3.420	0.240
O	3.535	0.267
HC	2.995	0.020

Appendix 2

Partial charges for AMBER, and in bracket for *pcff* force fields.

atoms	q	Ref.	atoms	q	Ref.	atoms	q	Ref.
C_1	–0.120	1	C_4	–0.180	1	O_2	–0.430	2
	(–0.106)			(–0.159)			(–0.531)	
H_1C_1	0.066	1	H_1C_4	0.066	1	C_5	0.160	2
	(0.053)			(0.053)			(0.066)	
H_2C_1	0.066	1	H_2C_4	0.066	1	H_3C_5	0.030	2
	(0.053)			(0.053)			(0.053)	
C_2	0.000	1	H_3C_4	0.066	1	H_1C_5	0.030	2
	(0.000)			(0.053)			(0.053)	
C_3	0.510	2	O_1	–0.330	2	H_2C_5	0.030	2
	(0.702)			(–0.396)			(0.053)	

1) W. L. Jorgensen et al., *J. Am. Chem. Soc.*, **118**, 11225(1996); 2) M. L. P. Price et al., *J. Comp. Chem.*, **22**, 1340 (2001)

Appendix 3

Parameters for bonding energetic term; a) for AMBER; b) for *pcff* force fields. For clarity, the mathematical expression is presented.

a) AMBER: $K\left(b-b_0\right)^2$

bonds	b_0 (Å)	k (kcal.mol^{-1}.Å^{-2})	Ref.
CT–CT	1.526	310.0	1
CT– C	1.522	317.0	1
CT–HC	1.090	340.0	2
CT–OS	1.410	320.0	1
C–O	1.229	570.0	1
C–OS	1.323	450.0	3

1) S.J. Weiner et al., *J. Comput. Chem.*, **7**, 230 (1986).
2) W. D. Cornell et al., *J. Am. Chem. Soc.* **117**, 5179 (1997).
3**) J.** Wang, et al., *J. Comput. Chem.*, **21**, 1049 (2000).

b) *pcff*: $K_2\left(b-b_0\right)^2+K_3\left(b-b_0\right)^3+K_4\left(b-b_0\right)^4$

bonds	b_0 (Å)	k_2 (kcal.mol^{-1}.Å^{-2})	k_3 (kcal.mol^{-1}.Å^{-3})	k_4 (kcal.mol^{-1}.Å^{-4})
CT–CT	1.53	299.67	–501.77	679.81
CT–C	1.5202	253.7067	–423.037	396.9
CT–HC	1.1010	345.0	–691.89	844.6
CT–OS	1.43	326.7273	–608.5306	689.0333
C–O	1.202	851.1403	–1918.4882	2160.7659
C–OS	1.3683	367.1481	–794.7908	1055.2319

Appendix 4

Parameters for valence energetic term; a) for AMBER/OPLS; b) for *pcff* force fields.

a) AMBER: $H\left(\theta-\theta_0\right)^2$

angles	θ_0 (deg)	h (kcal.mol^{-1}.deg^{-2})	Ref.
CT–CT–CT	109.50	37.0	1
CT–CT–C	111.10	63.0	3
HC–CT–HC	109.50	28.5	3
CT–CT–HC	109.50	37.0	1
CT–C–O	120.40	80.0	2
CT–C–OS	115.00	80.0	2
O–C–OS	125.00	80.0	2
C–OS–CT	117.00	60.0	1

1) S.J. Weiner et al., *J. Comput. Chem.*, **7**, 230 (1986).
2) J. Wang, et al., *J. Comput. Chem.*, **21**, 1049 (2000).
3) **J.** Wang, et al., *J. Comput. Chem.*, **22**, 1219 (2000).

b) *pcff*: $H_2(\theta-\theta_0)^2 + H_3(\theta-\theta_0)^3 + H_4(\theta-\theta_0)^4$

Angles	θ_0 (deg)	H_2 (kcal.mol^{-1}.deg^{-2})	H_3 (kcal.mol^{-1}.deg^{-3})	H_4 (kcal.mol^{-1}.deg^{-4})
CT–CT–CT	112.67	39.516	–7.443	–9.5583
CT–CT–C	108.53	51.9747	–9.4851	–10.9985
HC–CT–HC	107.66	39.641	–12.921	–2.4318
CT–CT–HC	110.77	41.453	–10.604	5.129
CT–C–O	123.145	55.5431	–17.2123	0.1348
CT–C–OS	100.318	38.8631	–3.8323	–7.9802
O–C–OS	120.797	95.3446	–32.2869	6.3778
C–OS–CT	113.288	61.2868	–28.9786	7.9929
OS–CT–HC	107.688	65.4801	–10.3498	5.8866

Appendix 5

Dihedral angle energetic term for AMBER, and in bracket for *pcff* force fields.

$$V_1\left[1-\cos\left(\phi-\phi_1^0\right)\right]+V_2\left[1-\cos\left(2\phi-\phi_2^0\right)\right]+V_3\left[1-\cos\left(3\phi-\phi_3^0\right)\right]$$

dihedral angles	V_1 (kcal.mol^{-1})	φ_1 (deg)	V_2 (kcal.mol^{-1})	φ_2 (deg)	V_3 (kcal.mol^{-1})	φ_3 (deg)	Ref.
CT–CT–CT–CT	0.22 (0.00)	180.0 (0.0)	0.34 (0.0514)	180.0 (0.0)	0.195 (–0.1430)	0.0 (0.0)	4
CT–CT–CT–C	0.00 (0.0972)	0.0 (0.0)	0.00 (0.0722)	0.0 (0.0)	0.1555 (–0.2581)	0.0 ()	2
HC–CT–CT–CT	0.00 (0.0000)	0.0 (0.0)	0.00 (0.0316)	0.0 (0.0)	0.155 (–0.1681)	0.0 (0.0)	4
HC–CT–CT–HC	0.00 (–0.1432)	0.0 (0.0)	0.00 (0.0617)	0.0 (0.0)	0.130 (–0.1083)	0.0 (0.0)	4
CT–CT–C–O	0.00 (0.0442)	0.0 (0.0)	0.00 (0.0292)	0.0 (0.0)	0.067 (0.0562)	180.0 (0.0)	1
CT–CT–C–OS	0.00 (1.8341)	0.0 (0.0)	0.00 (2.0603)	0.0 (0.0)	0.000 (–0.0195)	0.0 (0.0)	1
CT–OS–C–CT	0.00 (2.5594)	0.0 (0.0)	2.70 (2.2013)	0.0 (0.0)	0.000 (0.0325)	0.0 (0.0)	3
O –C –OS–CT	1.40 (0.0000)	180.0 (0.0)	2.70 (2.2089)	180.0 (0.0)	0.000 (0.0000)	0.0 (0.0)	4
C–OS–CT–HC	0.00 (0.0000)	0.0 (0.0)	0.00 (0.0000)	0.0 (0.0)	0.3833 (–0.1932)	0.0 (0.0)	1

1) S.J. Weiner et al., *J. Comput. Chem.*, **7**, 230 (1986).
2) W. D. Cornell et al., *J. Am. Chem. Soc.* **117**, 5179 (1997).
3) J. Wang, et al., *J. Comput. Chem.*, **21**, 1049 (2000).
4) **J.** Wang, et al., *J. Comput. Chem.*, **22**, 1219 (2000).

5 REFERENCES

[1] D. Rigby, H. Sun and B. Eichinger, Computer simulations of poly(ethylene oxide): force field, pvt diagram and cyclization behaviour, *Polym*. *Int*. **1997**, *44*, 311.

[2] N. L. Allinger, K. Chen and J. H. Lii, An improved force field (MM4) for saturated hydrocarbons, *J*. *Comput*. *Chem*. **1996**, *17*, 642.

[3] B. R. Gelin, *Molecular Modeling of Polymer Structures and Properties*, Hanser Publishers, Munich, 1994.

[4] U. M. Apel, R. Hentschke and J. Helfrich, Molecular dynamics simulation of syndio– and isotactic PMMA in benzene, *Macromolecules* **1995**, *28*, 1778–1785.

[5] A. Soldera, Comparison between the glass transition temperatures of the two PMMA tacticities: a mlecular dynamics simulation point of view, *Macromol*. *Symp*. **1998**, *133*, 21–32.

[6] A. Soldera, Energetic analysis of the two PMMA chain tacticities and PMA through molecular dynamics simulations, *Polymer* **2002**, *43*, 4269–4275.

[7] A. Soldera and Y. Grohens, Local dynamics of stereoregular PMMAs using molecule simulation, *Macromolecules* **2002**, *35*, 722–726.

[8] A. Soldera and Y. Grohens, Cooperativity in stereoregular PMMAs observed by molecular simulation, *Polymer* **2004**, *45*, 1307–1311.

[9] M. Tsige and P. L. Taylor, Simulation study of the glass transition temperature in polymethylmethacrylate, *Phys*. *Rev*. *E*. **2002**, *65*, 021805.

[10] S. B. Sane, T. Cagin, W. G. Knauss and W. A. Goddard, Molecular dynamics simulations to compute the bulk response of amorphous PMMA, *J*. *Comput*.*Aided Mat*. *Des*. **2001**, *8*, 87–106.

[11] F. Jensen, *Introduction to Computational Chemistry*, John Wiley & Sons, Chichester, 1999.

[12] J. R. Maple, M.–J. Hwang, T. P. Stockfisch, U. Dinur, M. Waldman, C. S. Ewig and A. T. Hagler, Derivation of class II force fields. 1. Methodology and quantum force field for the alkyl functional group and alkane molecules, *J*. *Comput*. *Chem*. **1994**, *15*, 162–182.

[13] E. Osawa and K. B. Lipkowitz. In: D. B. Boyd, D. B. Boyd. Reviews in Computational Chemistry, New York: VCH Publishers, Inc., 1995.

[14] D. A. Pearlman, D. A. Case, J. W. Caldwell, W. S. Ross, T. E. Cheatham III, S. DeBolt, D. Ferguson, G. Seibel and Kollman.P., AMBER, a package of computer programs for applying molecular mechanics, normal mode analysis, molecular dynamics and free energy calculations to simulate the structural and energetic properties of molecules, *Comp*. *Phys*. *Commun*. **1995**, *91*, 1–41.

[15] S. B. Sane, T. Cagin, W. G. Knauss and W. A. Goddard, Molecular dynamics simulations to compute the bulk response of amorphous PMMA, *J*. *Comput*.*–Aided Mat*. *Des*. **2002**, *8*, 87–106.

[16] W. L. Jorgensen and J. Tiraod–Rives, *J*. *Am*. *Chem*. *Soc*. **1988**, *110*, 1657.

[17] M. P. Allen and D. J. Tildesley, *Computer Simulation of Liquids*, Clarendon Press, Oxford, 1987.

[18] H. Meirovitch, Computer simulation of self_avoiding walks: testing the scanning method, *J*. *Chem*. *Phys*. **1983**, *79*(*1*), 502–508.

[19] D. N. Theodorou and U. W. Suter, Detailed molecular structure of a vinyl Polymer glass, *Macromolecules* **1985**, *18*, 1467–1478.

[20] M. Vacatello and P. J. Flory, Conformational statistics of poly(methyl methacrylate), *Macromolecules* **1986**, *19*, 405–415.

[21] W. Smith and T. R. Forrester, DL_POLY 2.14, *J*. *Molec*. *Graphics*. **1996**, *14*, 136.

[22] H. J. C. Berendsen, J. P. M. Postma, W. F. Van Gunsteren, DiNola, A. and J. R. Haak, Molecular dynamics with couplin to an external bath, *J*. *Chem*. *Phys*. **1984**, *81*, 3684–3690.

[23] H. C. Andersen, MD simulations at constant pressure and/or temperature, *J*. *Chem*. *Phys*. **1980**, *72*, 2384.

[24] M. Parrinello and A. Rahman, *J*. *Appl*. *Phys*. **1981**, *52*, 7182.

[25] D. Rigby and R. J. Roe, Molecular dynamics simulation of polymer liquid and glass. I. Glass transition., *J*. *Chem*.

Phys. **1987**, *87*(*12*), 7285–7292.

[26] N. C. Ekdawi–Sever, P. B. Conrad and J. J. de Pablo, Molecular simulation of sucrose solutions near the glass transition temperature, *J. Phys*. *Chem*. *A* **2001**, *105*, 734–742.

[27] A. V. Lyulin and M. A. J. Michels, Molecular dynamics simulation of bulk atactic polystyrene in the vicinity of Tg, *Macromolecules* **2002**, *35*, 1463–1472.

[28] R. H. Gee and R. H. Boyd, The role of the torsional potential in relaxation dynamics: a MD study of PE, *Comput*. *Theor*. *Polym*. *Sci*. **1998**, *8*, 91–98.

[29] C. F. Fan, T. Cagin, Shi W. and K. A. Smith, Local chain dynamics of a model polycarbonate near glass transition temperature: A MD simulation, *Macromol*. *Theory Simul*. **1997**, *6*, 83–102.

[30] J. Lub, F. C. B. M. Van Vroonhoven, D. Van Leyen and A. Benninghoven, *J*. *Polym*. *Sci*., *Part B: Polym*. *Phys*. **1989**, *27*, 2071.

Biographies

Armand Soldera is assistant professor of molecular–physical chemistry at the Université de Sherbrooke, Québec, Canada. After obtaining a Ph.D. degree in the study of ferroelectric liquid crystals under the direction of Dr. D. Guillon and Pr. J.F. Nicoud, Université Louis Pasteur, Strasbourg, France, he undertook postdoctoral research with Pr. R.E. Prud'homme and Pr. C.G. Bazuin, Université Laval, Québec, Canada. Thereafter, he worked for eight years as research engineer in charge of the molecular modeling of polymers, at the Commissariat à l'Energie Atomique, CEA, France. He is also associated professor at the Institut Supérieur des Matériaux et Mécaniques Avancés, ISMANS, France. Since 2002, his studies are devoted to a perpetual interaction between experience and molecular modeling to better understand specific properties, and thus to enable the design of new compounds with optimal properties.

Noureddine Metatla is a Ph.D. student under the supervision of Pr. A. Soldera at the Chemistry Department, Université de Sherbrooke, Québec, Canada. He presently works on the study of the difference in T_gs between stereoregular polymers by the use of molecular modeling of polymers. He received his B.Sc in Physics from the Annaba University, Algeria, and M.Sc. from the Nice Sophia Antipolis University, France.